AN EXPERIMENTAL INVESTIGATION OF THE INTERACTION BETWEEN A GLANCING SHOCK WAVE AND A TURBULENT BOUNDARY LAYER

ICAS-80-14.1

H. Kubota and J.L. Stollery
Cranfield Institute of Technology, Bedford, England.

ABSTRACT

A variable incidence wedge, mounted from the side of a supersonic tunnel, has been used to study 3-D glancing interaction. A wedge-generated oblique shock-wave interacts with the thick turbulent boundary layer growing along the tunnel side wall. Two related test programmes have been completed using a 6cm x 6cm intermittent tunnel and a 23cm x 23cm continuous tunnel, both operating at a Mach number of approximately 2.5. The experimental results include oil-flow pictures, vapour-screen and smoke photographs, surface pressure distributions, local heat transfer, liquid crystal pictures of surface temperature, and viscous layer surveys. The test data show that the interaction is complex, with an induced layer which originates near the root of the wedge, spreading and crossing the path of the side wall boundary layer. Separation is defined by the appearance of a complete convergence line in the surface-oil-flow pictures. No separation occurs as long as the surface stream lines are pliable enough to be bent along the edge of the induced layer, even when the surface flow deflection exceeds the shock angle. However, separation does take place when the induced layer forces the surface stream lines to deflect beyond a maximum permissible angle. A correlation of incipient separation data is given.

1. INTRODUCTION

The term 'glancing interaction' covers any flow in which an oblique shock wave generated by one surface, interacts with the boundary layer growing along another. Typical examples of glancing interaction occur at wing-body and tail-fin junctions, and in engine intakes. Two separate but related programmes are described here. In the 6cm x 6cm ($2\frac{1}{2}$in. x $2\frac{1}{2}$in.) tunnel a variable incidence wedge was mounted on the roof of the wind tunnel and spanned the test section. Hence there was a thick boundary layer on both the shock generator, and the side walls across which the shock glanced.

In the larger, continuous tunnel a variable incidence sharp-edged flat plate was mounted from the tunnel side wall as shown in figure 1. The model span was 80% of the test section width and the plate was mounted well above the floor in order to be clear of the boundary layer there. For both test programmes the Reynolds numbers were high enough for the boundary layers to be turbulent and no trips were used.

The objectives of the study were:

(i) to measure the pressure and heat transfer distributions over the side-wall interaction region,

(ii) to describe and understand the development of the flow field, particularly the boundary layer behaviour,

(iii) to define a separation criterion and relate it to the oblique shock strength causing the disturbance.

Notation

C equivalent thermal capacity per unit area of the calorimeter

Ch Stanton number

Ch_o Stanton number with no shock generator present (i.e. the flat plate value)

h heat transfer coefficient

h_a heat transfer coefficient, Pyrex to air (see figure 3)

h_b heat transfer coefficient, aluminium to Pyrex wall (see figure 3)

p static pressure

p_1 free-stream pressure, pressure far ahead of the interaction region

p_2 pressure behind the theoretical oblique shock wave (inviscid flow)

t time

T static temperature, ^oK

T_a air temperature (see figure 3)

T_{aw} adiabatic wall temperature

T_b temperature of aluminium backing plate (see figure 3)

T_g temperature of the Pyrex calorimeter (see figure 3)

T_o stagnation temperature

T_w wall temperature

X, Y cartesian co-ordinate system parallel and normal to the free-stream direction, origin at the leading edge of the shock generator

X_g, Y_g cartesian co-ordinate system along and normal to the wedge generator surface, origin at the leading edge

X_s, Y_s inviscid shock location in the X-Y plane

X_{gs}, Y_{gs} inviscid shock location in the X_g-Y_g plane

δ_i wedge angle for incipient separation

δ_s wedge angle-degrees

δ_o the 99.5% boundary layer thickness just upstream of the interaction region

2. THE EXPERIMENTAL PROGRAMMES

A list of the techniques used in each of the two test programmes (A and B) is given in Table 1. The working section test conditions are given in Table 2.

Table 1 Test Programmes

A 6 cm x 6 cm Intermittent Tunnel

B 22 cm x 22cm Continuous Tunnel

Techniques used:

Schlieren	A, B
Surface oil flow	A, B
Vapour screen	A, B
Smoke	B
Surface static pressure	A, B
Surface heat transfer	
Copper slug-calorimeter gauges	A
Pyrex " "	B
Boundary layer probe survey	
- upstream boundary layer	A, B
- region downstream of the shock	A
Encapsulated liquid crystal technique	A

Table 2 Test Conditions

Programme A

Mach No.	2.4	
Reynolds No.	1.0×10^7/m	(2.5×10^5/in)
Initial boundary layer conditions		
- 99.5% thickness	5mm	(0.2in)
- displacement thickness	2mm	(0.07in)
- momentum thickness	0.4mm	(0.015in)
Stagnation pressure	720mm Hg	(14psi)
Stagnation temperature	$\simeq 290^\circ$K	

Programme B

Mach No.	2.3	
Reynolds No.	0.3×10^7/m	(0.8×10^5/in)
Initial boundary layer conditions		
- 99.5% thickness	15mm	(0.6in)
- displacement thickness	4mm	(0.15in)
- momentum thickness	1mm	(0.04in)
Stagnation pressure	200mm Hg	(4psi)
Stagnation temperature	$\simeq 290^\circ$K	

3. EXPERIMENTAL TECHNIQUES

Many of the techniques employed were fairly standard and a very full account of all the methods used is given in Ref.1. Hence only an abbreviated account is given here.

3.1 Oil Flow Pictures

A mixture of titanium dioxide suspended in motor oil was used with a drop of oleic acid added to prevent coagulation of the titanium dioxide. The surface flow pictures were usually taken through the glass windows while the tunnel was still running.

3.2 Vapour-Screen Pictures

The vapour was formed from water, sucked directly into the settling chamber. Illumination was by a 250w slide-projector.

3.3 Static-Pressure Measurements

About two hundred side wall pressures had to be measured so a scani-valve system was used feeding a diaphragm-type pressure transducer. The readings were automatically printed out by a data-logger.

3.4 Heat-Transfer Measurements

In the small intermittent tunnel a slug-calorimeter was used (kindly loaned to us by Princeton University). Details of the instrument and the intended method of use are given in the paper by Oskam et.al.(Ref.2). The unit supplied had three calorimeters mounted flush in a 50mm dia. disc. The slugs are initially heated by a tiny jet of hot air to a temperature typically 20°K above the tunnel wall temperature which in turn is about 20°K above the adiabatic wall temperature. When the tunnel starts the hot jet is stopped, the slug cools rapidly, through the wall temperature, towards the adiabatic wall temperature. The slug cools rapidly since its thermal capacity is much smaller than that of the tunnel wall, from which the slug is of course insulated. In practice we found that the initial heating caused interference between the three slugs due to convection. A modified technique was adopted as described in Ref.3 by Davenport. Even then the accuracy of the results was not good and the size of the plug in which the three slugs were mounted prevented us from attaining the resolution required. The poor accuracy was primarily due to the small value of the 'driving' temperature difference available ($T_w - T_{aw}$). Thus relatively small changes of T_w with time, and of T_{aw} with position, significantly changed the driving temperature from the constant value assumed in reducing the data.

The Princeton slug calorimeter could have been used in the larger continuous tunnel (by suddenly altering the cooling water flow to the tunnel and hence the stagnation temperature of the air). However in the light of our earlier experience it was decided to adopt a somewhat novel Pyrex slug-calorimeter technique. About 60 thin-film, platinium-resistance thermometers were sputtered on a Pyrex glass plate in the usual way. The complete model is shown in fig.2. By operating the cooler at maximum conditions it was possible to hold T_o about 20°K below T_w (room temperature). The thin film to be used was first employed as a heater by passing a steady current of about 30mA through it. Thus a certain volume of the plate in the neighbourhood of the gauge was heated to around 5° above the reference wall temperature as shown in fig.3. The current was then reduced to 3mA and the gauge operated in the usual way as a thermometer measuring the time-temperature history of the local volume of substrate which acts as a calorimeter. By comparing the temperature record with the corresponding history for wind-off conditions the heat transfer coefficient can be obtained. With reference to fig.3 the heat balance is

$$C\frac{dT_g}{dt} = h_b(T_b - T_g) - h_a(T_g - T_a). \quad (1)$$

Assuming that the heat transfer coefficients, h_a and h_b, are independent of temperature and that T_a and T_b are independent of time then equation (1) may be re-written as

$$C\frac{dT_g}{dt} + (h_a + h_b)(T_g - T_a) = h_b(T_b - T_a) , \quad (2)$$

where the right hand side is now independent of t. The appropriate solution is

$$\frac{T_g - T_w}{T_{g_i} - T_w} = \exp - \frac{h_a + h_b}{C} . t ,$$

where T_{g_i} is the initial value of T_g.
A plot of T_g (t) will therefore provide $(h_a + h_b)/C$ where C is known and h_b can be obtained from wind off measurements. Full details are given in Ref.1.

3.5 The Encapsulated Liquid Crystal Technique

Liquid crystals were used in an attempt to visualise the global temperature distributions on the side wall surface (in the intermittent tunnel only). A number of different surface materials were used but hardboard, painted black, was the most successful. The crystals, diluted with an equal amount of hot water, were sprayed on the hardboard and allowed to dry. When the tunnel was started the air began to cool the board surface, and the crystals responded to the local surface temperatures by displaying colour patterns changing with time. Colour pictures were taken at various times during the typical ten second running time using a motor-driven camera.

3.6 Viscous Layer Surveys

Small individually designed probes were made to measure pitot pressure, static pressure and yaw-angle. For yaw a double tube probe was used with the open ends chamfered at 45^o. A probe drive system allowed the probes to be moved normally to the wall surface and pitched to align them with the local flow direction.

4. EXPERIMENTAL RESULTS

In many ways programme A acted as a pilot study for the main programme (B). Hence in this paper we concentrate on the measurements made in the larger, continuous, wind-tunnel.

4.1 Oil Flow Pictures

Oil flow pictures taken on both the side-wall and wedge-generator surfaces are shown in figs. 4, 5, 6 and 7, for wedge angles of between 7^o and 15^o. Concentrating for the moment on the side wall pictures it is obvious, even for $\delta_s = 7^o$, that the upstream influence of the shock is large, with the surface lines bending upwards far ahead of the 'inviscid shock' position (i.e. the position of the oblique shock wave in the free stream). However the surface streamlines do pass 'through' the shock position and move off downstream. Still on the side wall but very close to the corner the surface streamlines diverge (see the divergence line marked on the picture) and this is an early indication of a vortex tucked in the wall-wedge junction. Above this divergence line the surface streamlines move upwards converging very gradually with other surface streamlines that have penetrated the shock position. This convergence is more marked at $\delta_s = 10^o$ and all the surface streamlines now lie at an angle greater than the shock angle, with an 'incomplete convergence' line (i.c.) separating surface streamlines originating upstream of the shock from those originating from below. At $\delta = 13^o$ the convergence between the two flows is striking. A curved 'complete convergence' line lies like a 'bow wave' ahead of the wedge. Into this line surface streamlines from both upstream and downstream 'disappear'. This implies that material once very close to the surface, has moved away from the surface and thus we have *defined* separation by *the appearance of a complete convergence line* (marked CC on the photographs).

Again at $\delta_s = 15^o$ the most dominant feature in the oil flow picture is the CC line running from near the leading edge of the wedge, right across the side wall to interact with the roof of the tunnel. On the shock generator surface, near the corner, another convergence line is clearly visible and at a similar distance from the corner but on the side wall it is just possible to see a divergence line. These lines confirm the existence of a corner vortex. Flow initially passing over the wedge 'lifts off' and rolls over the vortex onto the side wall. Some flow enters the corner vortex itself but the rest moves up and across the tunnel side wall. However a close study of fig.7 (and also fig.6) shows yet another important flow feature. The surface oil lines which do 'escape' the corner vortex and move up the side wall (towards the calculated inviscid shock position, see fig.7) form an 'S' shaped pattern suggestive of some kind of spiralling flow close to the wall. The pictures also suggest that flow becomes more sluggish as the CC line is approached. Our interpretation of these complex patterns is given later but the driving mechanism is clearly the high pressure on the wedge generator trying to 'escape up the side wall' and the side wall pressure in turn trying to 'escape' forwards through the boundary layer.

The surface oil flow patterns on the wedge generator are also quite complex and are associated primarily with the shock shape formed by the interaction of the oblique-shock and the thick side-wall boundary-layer near the leading-edge-root region. The wedge surface is not considered further here since it was not the main area of interest. Further discussion of this region is however made in Ref.1.

4.2 Pressure Distributions

Isobar patterns are shown in fig.8 for three typical wedge angles. The most interesting feature is that the isobar pattern is roughly 'conical' in nature, particularly at the larger wedge angles. It is also obvious that the pressure propagates far upstream of the inviscid

shock position and that the CC (separation) line is near the forefront of the pressure rise. Fig.9 demonstrates the same features in another way, the pressure distributions being measured along lines parallel to the wedge generator surface. The zero position is the calculated station for the inviscid shock wave, the large upstream influence is therefore immediately evident. The inviscid pressure rise is also marked on the figures. Away from the corner the pressure takes a considerable distance over which to reach the final inviscid value. Fig.9 shows that the total pressure rise at $\delta_s = 7^o$ is gradual over the whole interaction region but at the larger wedge angles ($\delta_s = 10^o$ and 13^o) the pressure rise is made in two distinct steps. The pressure rises quickly in the neighbourhood of the convergence line, then tends to level out before rising again to the required inviscid level. These patterns are reminiscent of two dimensional separated flow, where the separated zone is characterised by a 'plateau' in the pressure distribution.

This two-step pressure pattern has been found in similar studies elsewhere (e.g. Ref.4) and fig.10 compares some measurements at M = 6 with the current study. In each case a convergence line had already appeared in the flow pattern (the position of the convergence line is marked on fig.10) and in each case the line precedes a pressure plateau region.

4.3 Heat Transfer Distribution

Lines of constant Ch over the whole side wall area are plotted in fig.11. At 7^o fig.11a shows no region of high heat transfer. At 10^o the pattern is complex (fig.11a) with two regions of high Ch , one near the convergence line, the other near the corner. The latter is probably associated with the attachment line of the corner vortex. These two zones persist at $\delta_s = 13^o$ (fig.11b). Although the overall pattern begins to look more conical, the important influence of the wedge leading-edge root-region distorts the picture. Taking vertical slices through fig.11c gives the distribution shown in fig.12. Looking at the distribution from top to bottom the first increase in Ch is associated with the oil flow lines crowding together and the pressure rising. It lies just ahead of the convergence (separation) line. The major peak in Ch lies near the corner and is clearly associated with corner vortex. In between these peaks the local value of Ch/Ch_o does rise to > 1.5 in what we believe to be a weak vortical region following separation.

Fig.12 also shows the results of two other studies (Refs.5 and 6) which show similar distributions where convergence lines have already appeared in the flow patterns.

4.4 Vapour Screen and Smoke Pictures

Fig.13 shows a selection of vapour screen pictures recording vertical slices of the flow field for $\delta_s = 13^o$. The pictures are not easy to interpret but the curvature of the shock as it approaches the wall is clearly visible together with some suggestion of bifurcation. The shape of the shock matches the calculated and measured shock position in the freestream (see right hand side of the pictures) and is near the measured convergence line position at the wall. There is a reasonably clear indication of a corner vortex in most of the pictures and some indication of the side-wall boundary layer thickness can be obtained. At the smaller wedge angles the vapour screen pictures were less interesting and are not shown here. However even at $\delta_s = 7^o$ there is clear evidence of a corner vortex.

To try to improve the flow visualisation, smoke was injected at various points through the wedge and side wall surfaces. Two of the most successful pictures are shown in fig.14 together with our interpretation. Fig.14b is the clearest evidence we have of the weak vortical separated layer following the convergence line.

5. THE PATTERN OF FLOW DEVELOPMENT

From all the evidence available it has been possible to construct the patterns shown in figs. 15 and 16.

For quite modest wedge angles a corner vortex forms and in fig.15 this is an accepted feature of an otherwise attached flow field. Our interpretation of the various flow pictures, plus the pressure and heat transfer distributions, leads to a double viscous layer model in which part of the wedge boundary layer pushes its way under the side wall boundary layer as shown in fig.15. In this way the side wall surface streamlines can be deflected, through quite large angles, towards an incomplete convergence line which marks the extent to which the wedge boundary layer has infiltrated. Fig.15 is meant to be indicative of flows up to $\delta_s = 10^o$ in this investigation.

For larger wedge angles the adverse pressure gradient becomes too severe for the side wall boundary layer and it separates. A complete convergence line forms in the oil flow pattern and a plateau develops in the pressure distribution. The flow where the two viscous layers are in contact is highly skewed and they partly roll up to form a weak vortex (above the corner vortex) as indicated by the smoke pictures. The oil flow pictures and the modest rise in heat transfer in the middle of this zone support this description and fig.16 is thought to represent the flows at wedge angles equal to or greater than 13^o in our study.

It must be emphasised that both the corner vortex and the weak vortical separated layer postulated above, were of similar size to the boundary layer thickness (δ_o) in our investigation. However if the longitudinal scale of the model could have been increased then presumably the vortex flows would have grown and could have greatly exceeded the local value of δ_o instead of lying buried within it.

6. A CRITERION FOR INCIPIENT SEPARATION

There are, unfortunately, two different criteria for determining the incipient separation condition for a turbulent boundary layer interacting with a skewed shock.

The first is due to McCabe (Ref.7). McCabe accepted Maskell's definition of a separation line (Ref.10) as an envelope of the limiting streamlines at the surface, but in McCabe's experiments these lines were formed roughly parallel to the shock. He therefore assumed that *incipient separation occurred when the surface flow turned parallel to the inviscid shock wave direction.* McCabe developed a simple approximate theory by assuming that the vorticity in the boundary layer is convected through an oblique shock wave with the velocity of the local external flow. This enabled him to relate the flow deflection angle at the surface to that at the edge of the boundary layer. Then by equating the surface flow deflection angle to the shock wave angle, the wedge angle for incipient separation (δ_i) could be calculated.

Korkegi (Ref.8) showed that at high Mach numbers, McCabe's criterion could be approximated by the very simple relation $M\delta_i = 0.364$ (assuming $\gamma = 1.4$). However at that time (1973) Korkegi found that the best agreement with experiment was obtained by changing the constant to 0.3. McCabe's criterion has the advantage that it is *relatively* easy to measure experimentally, when the surface oil pattern has turned through the wave angle. By 1975 more data were available and Korkegi (Ref.9) confirmed that the simple correlation,

$$M\delta_i = 0.3 ,$$

was in good agreement with the experimental data over the range $2 < M < 6$. The relevant figure from Ref.9 is re-drawn in fig.17a and our own data added. Both McCabe's and Korkegi's calculated values are also shown, together with the wedge angle for shock detachment.

Since McCabe's tests many others have been performed. They showed that it was often possible to deflect the surface flow through angles *exceeding* the shock wave angle before a separation line was formed. Hence a second criterion was derived directly from the 'ordinary separation' model of Maskell (Ref.10). If a three dimensional flow separates then part or all of it leaves the surface. Streamlines that were on the surface 'disappear', and separation occurs along a convergence line into which the surface streamlines merge. According to Maskell's model the surface streamlines should enter from both sides of the separation line. However, Lighthill in Ref.14 considered the mass flux through a rectangular streamtube adjacent to the surface. If the surface streamlines converge then the height of the rectangle must increase rapidly as the separation line is approached and eventually the flow 'lifts off'. From this simple argument it is clear that a complete convergence with streamlines entering from just one side is an adequate definition of separation.

This description is physically more realistic, and is the one we have adopted. *Thus incipient separation is defined by the first formation of a complete convergence line.* Below incipient separation any oil 'line' that forms will widen along its length to become more of a wedge-shaped region, rather than a line. Conversely, in a well separated flow, it may be possible to see streamlines entering the narrow convergence line from both sides. In practice, the interpretation of oil flow pictures needs care. The oil pattern is determined by many forces, including surface tension and buoyancy, as well as skin friction and pressure gradient. The reaction of the oil film to these forces is in turn dependent on some of the properties of the oil mixture used, such as density and viscosity. The difficulties of interpretation are probably responsible for most of the scatter in the experimental data (see figs. 17a and 17b).

Our experiments show, like many of those before us, (e.g. Refs. 2 and 5) that the surface flow can be turned through angles considerably in excess of the wave angle before a complete convergence line is formed. Hence the values of δ_i measured using this criterion are greater than those measured using the ideas of McCabe. The data are shown in fig.17b.

Comparing figs. 17a and 17b it is obvious that the second criterion increases the value of δ_i particularly at high Mach numbers. If anything the data support the contention of Goldberg (Ref.11) that δ_i varies little with Mach number, a very rough value being 8°.

7. FINAL REMARKS

The glancing shock interaction studied here comprises two viscous layers:

(a) the side-wall boundary layer,

(b) an induced layer coming from the shock generator surface near the root.

The induced layer crosses the path of the side-wall boundary layer and pushes up underneath it.

As long as the surface streamlines of the side-wall boundary layer are pliable enough to bend along the edge of the induced layer, no flow separation occurs even if the surface flow deflection exceeds the 'inviscid' shock angle. However an ordinary separation does occur when the induced layer forces the side-wall surface streamlines to bend beyond a maximum permissible angle. They then coalesce into a complete convergence line, lift off from the surface and roll over and around the induced flow below.

A complex but consistent flow pattern development is described which explains the evolution of the measured pressure and heat-transfer distributions.

A correlation of incipient separation data (defined by the appearance of a complete convergence line) is presented. The correlation is compared with those given earlier by Korkegi and McCabe.

8. REFERENCES

1. Kubota, H. Investigation of three-dimensional shock wave boundary layer interactions. College of Aeronautics Report 8001 (AFOSR-76-3006), January 1980.

2. Oskam, B.
Vas, I.E.
Bogdonoff, W.J.
Oblique shock wave boundary layer interactions in three dimensions at Mach 3.
AFFDL TR-76-48, Part I, January 1976
AFFDL TR-76-48, Part II March 1978.

3. Davenport, N.C.
Heat transfer in a region of glancing shock wave boundary layer interaction.
College of Aeronautics Memo 7806, July 1978.

4. Kaufman, L.G.
Johnson, C.B.
Pressure distributions induced by elevon deflections on swept wings and adjacent end-plate surfaces at Mach 6.
NASA TM X-3470, April 1977.

5. Neumann, R.D.
Token, K.H.
Prediction of surface phenomena induced by three dimensional interactions on planar turbulent boundary layers. International Astronautical Federation Paper 74-058, October 1974.

6. Johnson, C.B.
Kaufman, L.G.
Heat transfer distributions induced by elevon deflections on swept wings and adjacent surfaces at Mach 6.
NASA TM 74045 August 1978.

7. McCabe, A.
The three-dimensional interaction of a shock wave with a turbulent boundary layer.
The Aeronautical Quarterly, Vol.17, Part 3, pp 231-252, August 1966.

8. Korkegi, R.H.
A simple correlation for incipient turbulent boundary layer separation due to a skewed shock wave.
AIAA Journal, vol.11, no.11 pp 1578-1579, November 1973.

9. Korkegi, R.H.
Comparison of shock-induced two and three dimensional incipient turbulent separation.
AIAA Journal, vol.13, no.4, pp 534-535, April 1975.

10. Maskell, E.C.
Flow separation in three dimensions.
RAE Report, Aero.2565, November 1955.

11. Goldberg, T.J.
Three dimensional separation for interaction of shock waves with turbulent boundary layers.
AIAA Journal, vol.11, no.11, pp 1573-1575, November 1973.

12. Peake, D.J.
Three dimensional swept shock/turbulent boundary layer separations with control by air injection.
NRC Aero Rpt.LR-592, 1976.

13. Stanbrook, A.
An experimental study of the glancing interaction between a shock wave and a turbulent boundary layer.
ARC CP 555, July 1960.

14. Lighthill, M.J.
Attachment and separation in three-dimensional flow.
Section II, §2-6, pp.72-82,of "Laminar Boundary Layers"
Ed. Rosenhead, L.
Oxford University Press, 1963.

9. ACKNOWLEDGEMENTS

It is a pleasure to record our debt to Mr. S.W. Clark and his staff, of the Aerodynamics Workshop for their help in the experimental study. Most of this work was generously supported by the U.S. Air Force through its European Office of Aerospace Research and Development in London. The Contract Monitor was Mr. Richard Neumann of the Wright Aeronautical Laboratories, Wright Patterson AFB, Ohio, U.S.A.

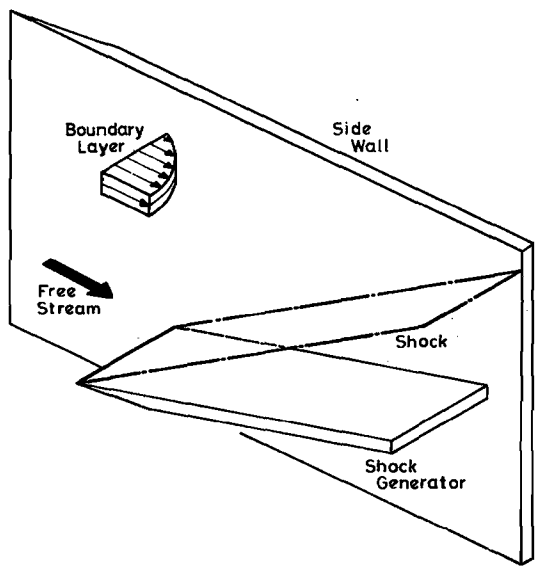

Fig. 1 Glancing Shock Boundary-Layer Interaction, Model B

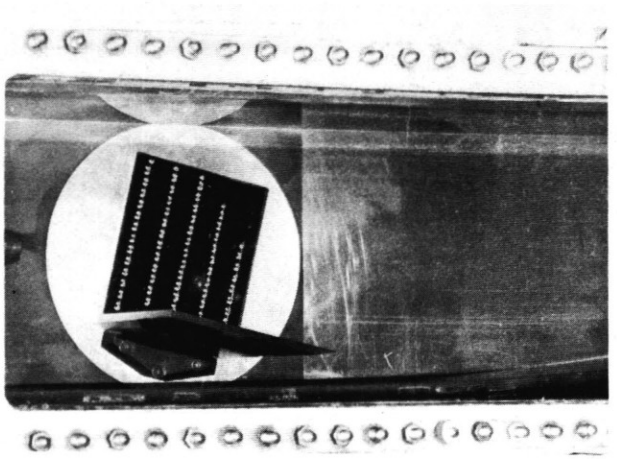

Fig. 2 The Heat Transfer Model for Programme B

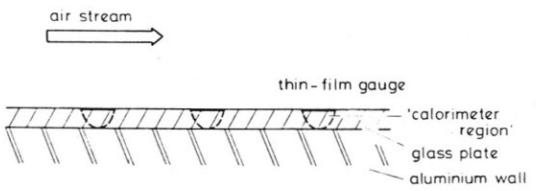

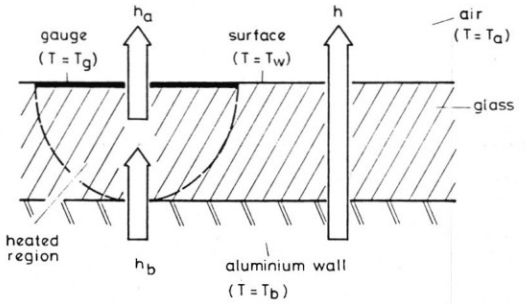

$$C\frac{dT_g}{dt} + (h_a + h_b)(T_g - T_a) = h_b(T_b - T_a)$$

$$\frac{T_g - T_w}{T_{g_i} - T_w} = \exp\left(-\frac{h_a + h_b}{C}\,t\right)$$

i: initial

Fig.3 Quasi-Transient Thin-Film-Gauge Calorimeter Technique (Pyrex Slug)

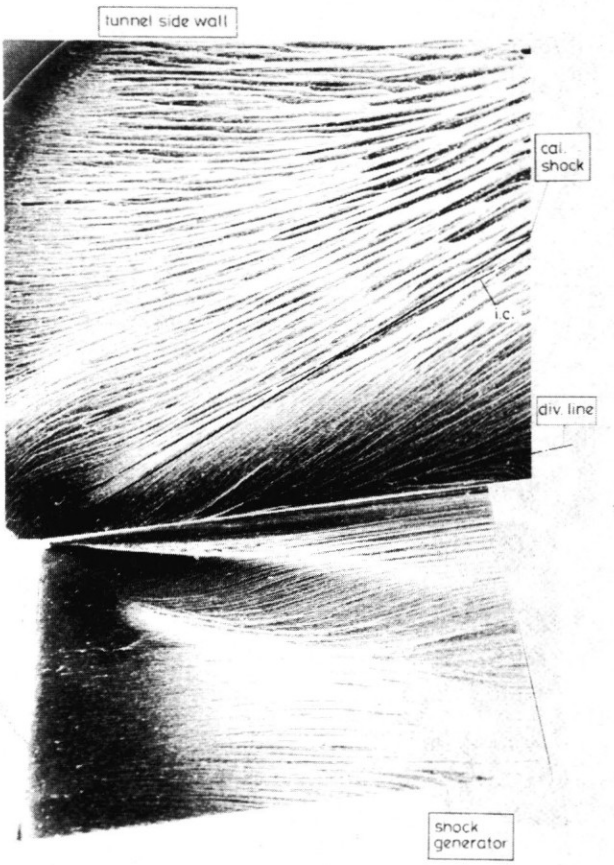

Fig. 4 Oil-Flow Picture at $\delta_s = 7^o$

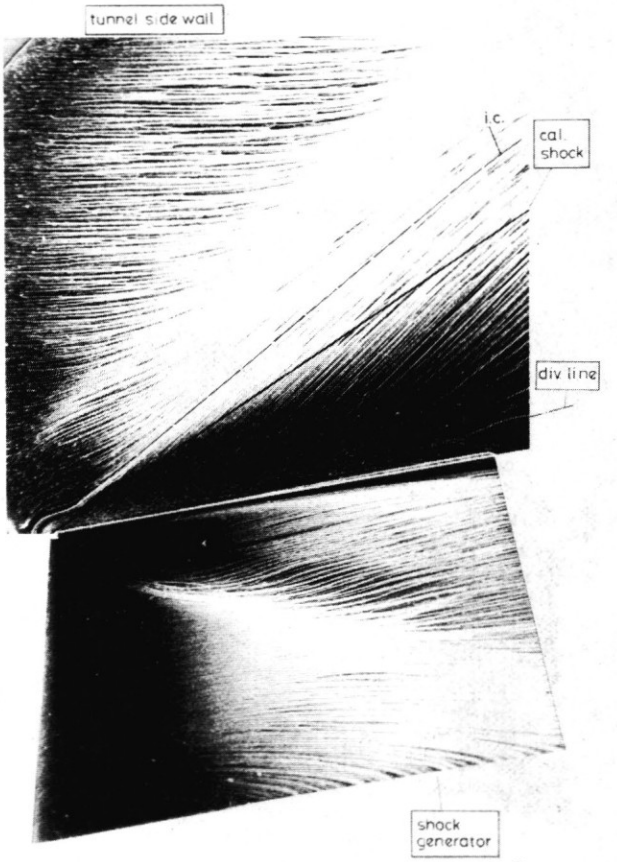

Fig. 5 Oil-Flow Picture at $\delta_s = 10^o$

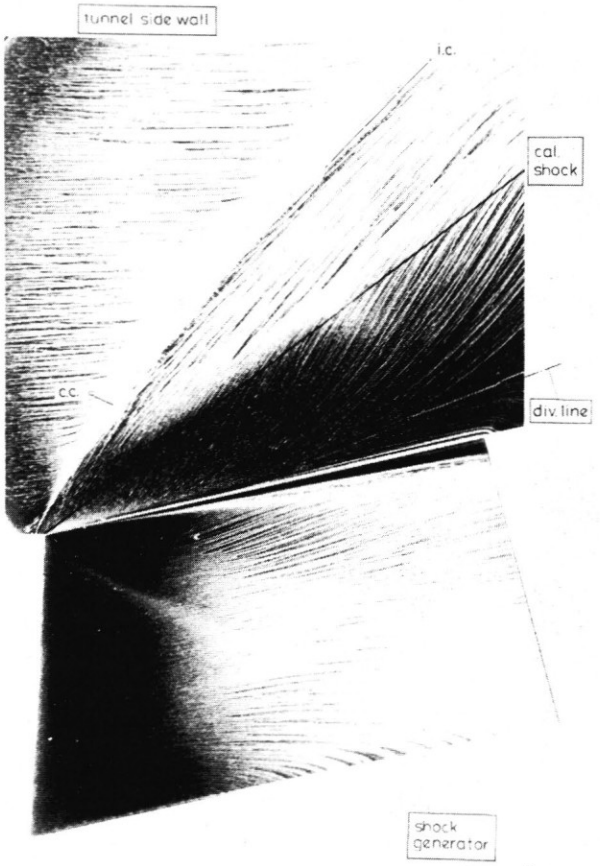

Fig. 6 Oil-Flow Picture at $\delta_s = 13^o$

Fig. 7 Oil-Flow Picture at $\delta_s = 15^o$

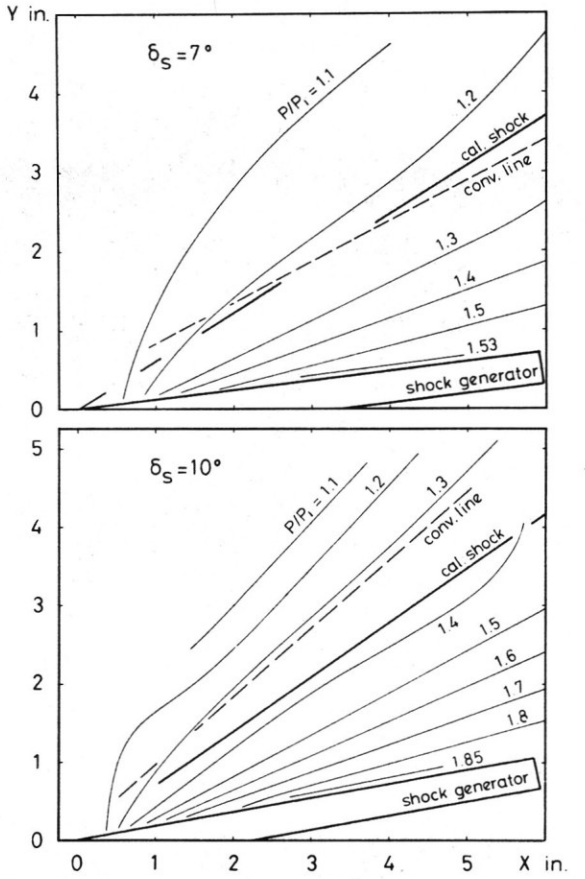

Fig. 8(a) Wall-Surface Isobars - Attached Flow

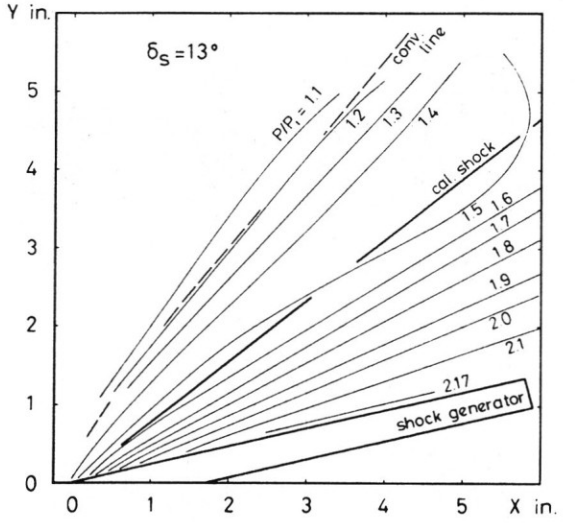

Fig. 8(b) Wall-Surface Isobars - Separated Flow

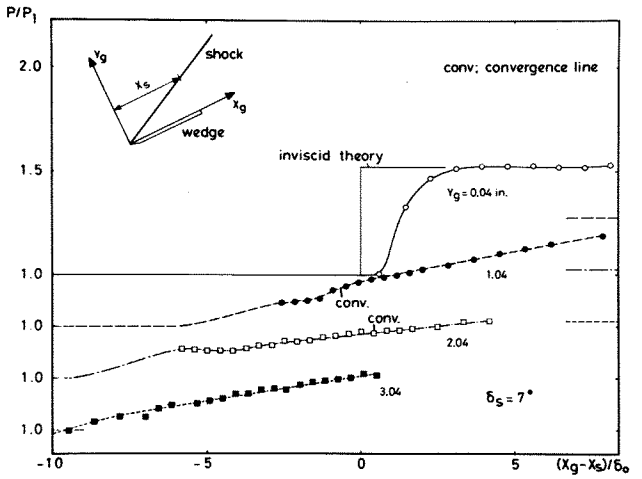

Fig. 9a $\delta_s = 7^o$

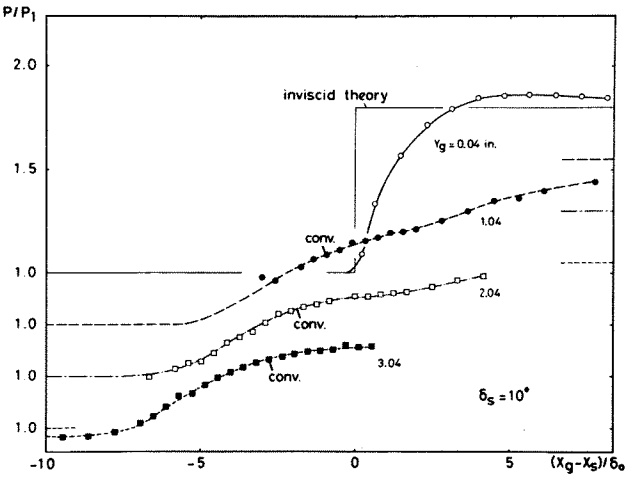

Fig. 9b $\delta_s = 10^o$

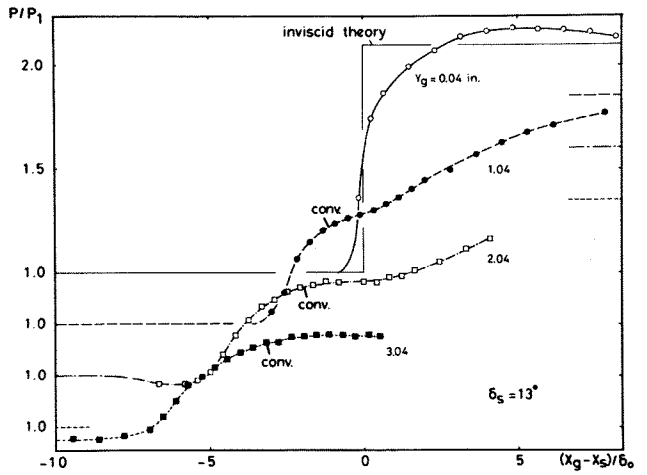

Fig. 9c $\delta_s = 13^o$

Fig. 9 Wall-Surface Pressure Distributions

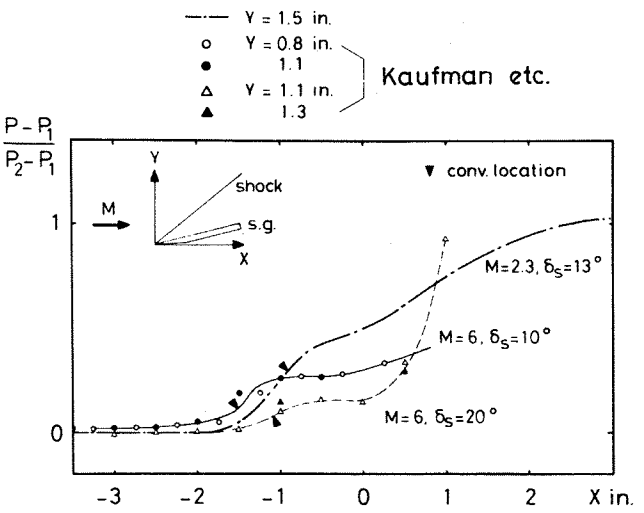

Fig. 10 Wall-Surface Pressure Distributions - Comparison with Other Results

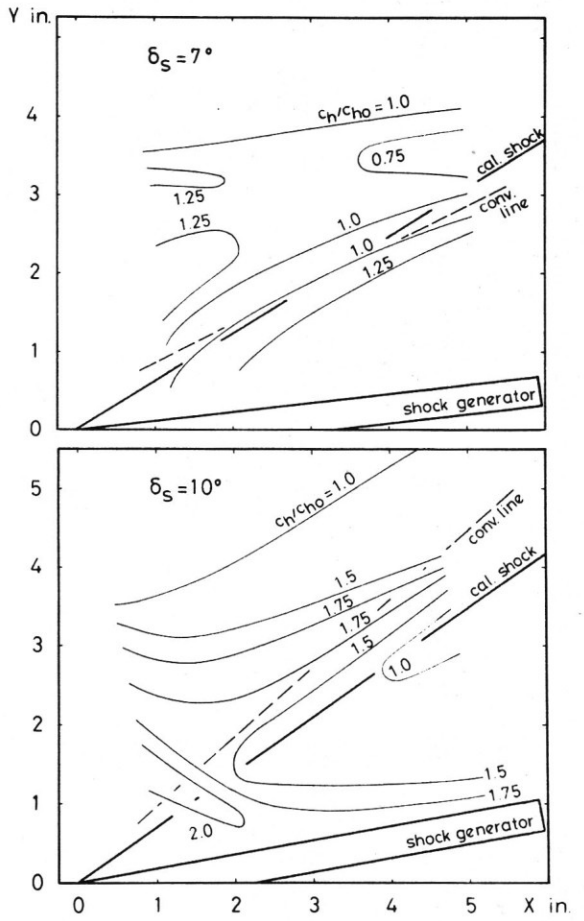

Fig. 11(a) Heat Transfer Distributions
- Attached Flow

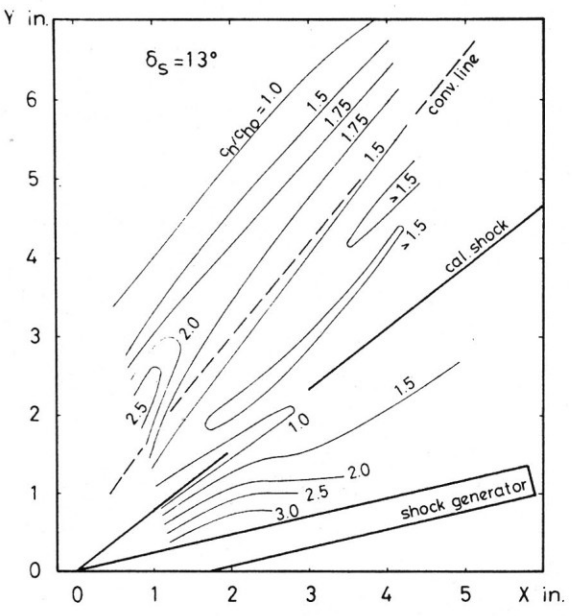

Fig. 11(b) Heat Transfer Distributions
- Separated Flow

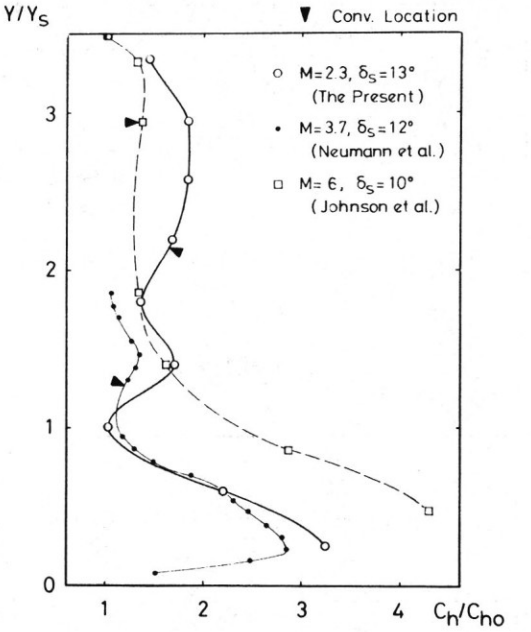

Fig. 12 Heat Transfer Patterns
- Comparison with Other Data

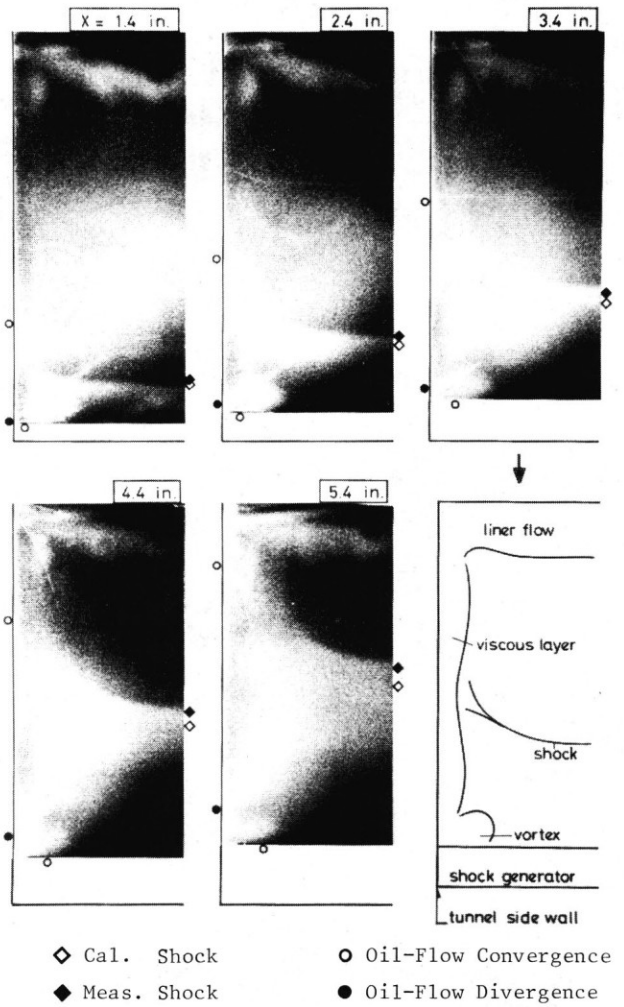

Fig.13 Vapour-Screen Pictures at $\delta_s = 13^o$

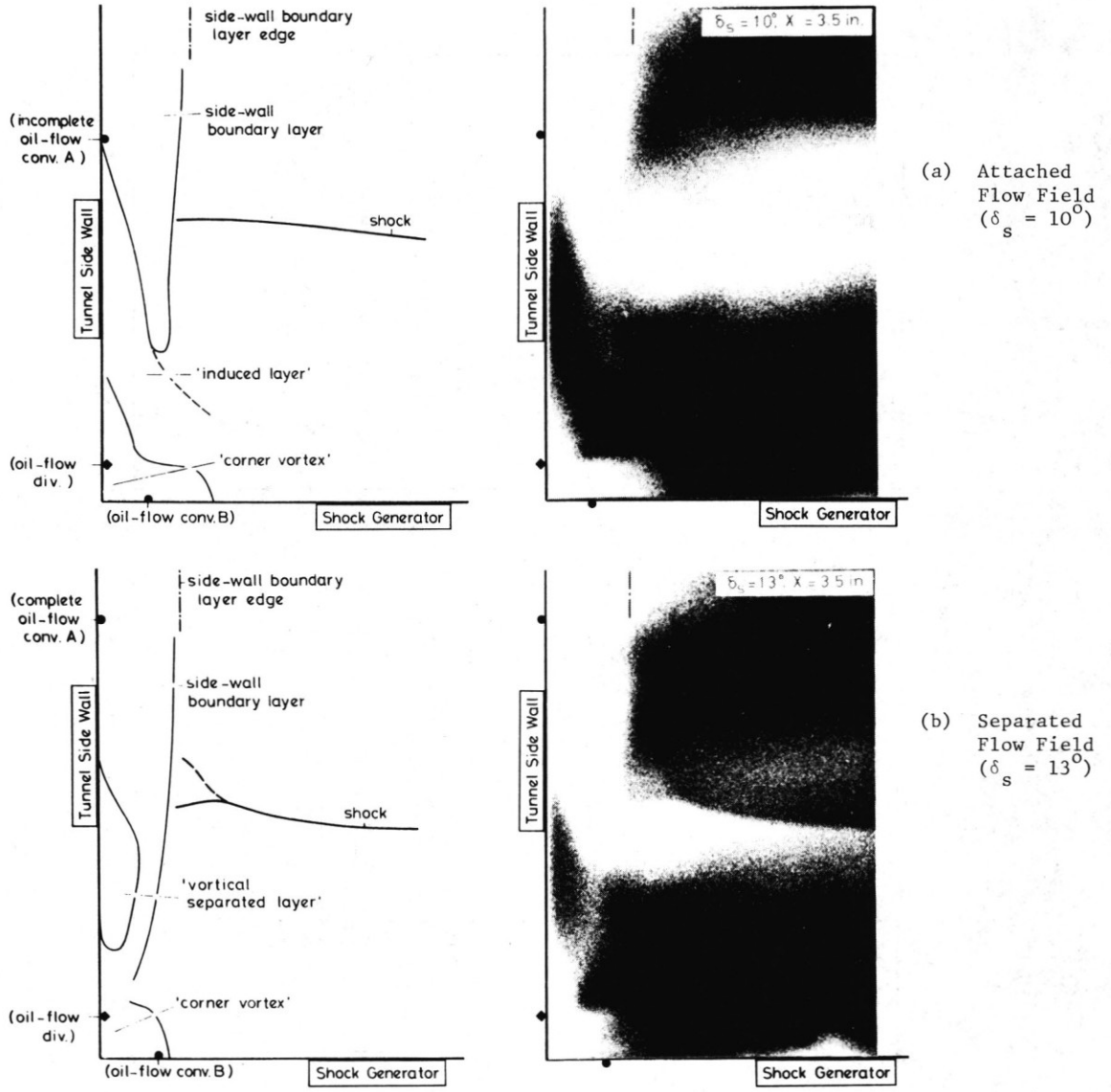

Fig. 14 Smoke and Vapour-Screen Pictures, Sectional Views taken from Upstream

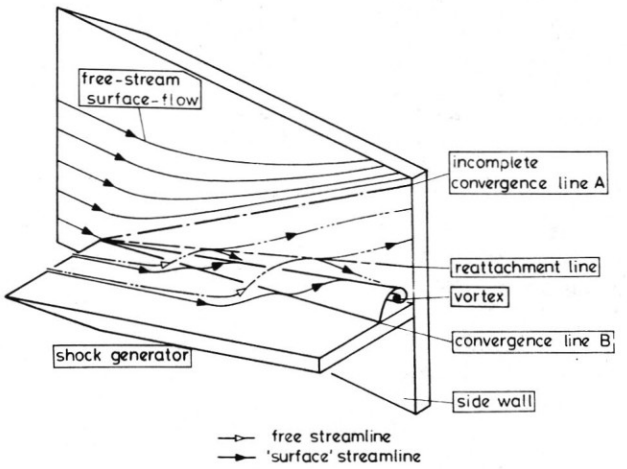

Fig. 15 Attached Flow-Field Model

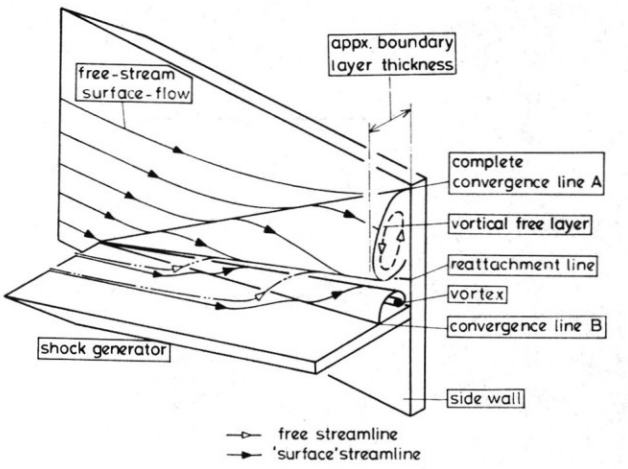

Fig. 16 Separated Flow-Field Model

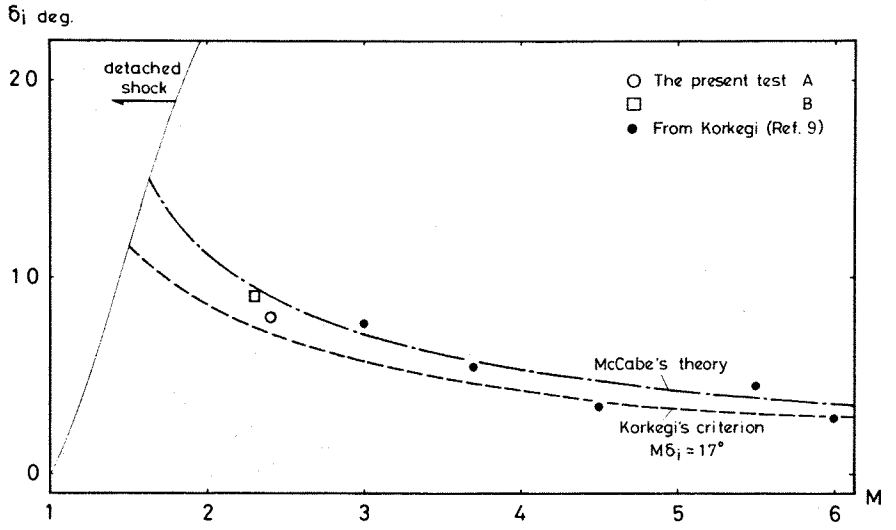

Fig. 17a The Wedge Angle to Induce Incipient Separation - As Defined by McCabe's Criterion

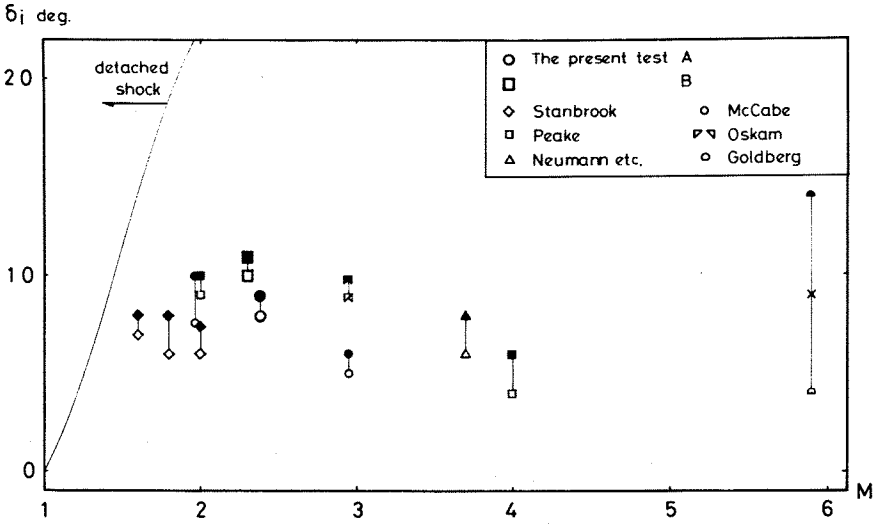

Fig. 17b The Wedge Angle to Induce Incipient Separation - As Defined by the Formation of a Complete Convergence Line